Heat capacity of RFe_xMn_{12-x} (R = Gd, Tb and Dy) compounds: wiping out a cooperative 4f–4f exchange interaction by breaking the 3d–4f magnetic symmetry

2008 J. Phys.: Condens. Matter 20 345203

(http://iopscience.iop.org/0953-8984/20/34/345203)

J. Phys.: Condens. Matter **20** (2008) 345203 (9pp) doi:10.1088/0953-8984/20/34/345203

Heat capacity of RFe_xMn_{12-x} (R = Gd, Tb and Dy) compounds: wiping out a cooperative 4f–4f exchange interaction by breaking the 3d–4f magnetic symmetry

C Piqué[1], J A Blanco[1], R Burriel[2], E Abad[1], J Fernández-Rodríguez[3] and M Artigas[2]

[1] Departamento de Física, Universidad de Oviedo, Campus de Viesques, E-33204 Gijón, Spain
[2] Instituto de Ciencia de Materiales de Aragón (CSIC–Universidad de Zaragoza), E-50009 Zaragoza, Spain
[3] European Synchrotron Radiation Facility, BP 220, F-38043 Grenoble Cedex, France

E-mail: pique@uniovi.es

Received 28 April 2008, in final form 21 July 2008
Published 1 August 2008
Online at stacks.iop.org/JPhysCM/20/345203

Abstract

Using adiabatic calorimetry the heat capacity of a series of RFe_xMn_{12-x} (R = Gd, Tb and Dy) compounds has been measured from 3 to 350 K. The substitution of Fe for Mn in RFe_xMn_{12-x} influences both the magnetic interactions on the 3d sublattice and the magnetism of R (the Néel temperature doubles on going from $x = 0$ to 6 and the compounds become ferromagnetic for $x = 8$ with Curie temperatures of around 300 K). In pure $TbMn_{12}$ the heat-capacity data shows a λ-type anomaly associated with the independent cooperative magnetic ordering of the R sublattice (∼5 K), while the anomaly related to the Mn magnetic ordering (∼100 K) is rather smooth, as observed in other itinerant magnetic systems such as YMn_{12}. In contrast, the substitution of Fe for Mn leads, on the one hand, to a more localized magnetic behaviour of the 3d sublattice, and, on the other, to magnetic polarization effects between the 3d and 4f sublattices, together with the disappearance of the cooperative magnetic ordering of the R sublattice due to the breaking of the antiferromagnetic symmetry in the 3d sublattice. This is reflected in the heat-capacity curve through a smooth Schottky-like anomaly. In the case of Gd compounds the magnitude of the exchange molecular-field parameter has been deduced by fitting the magnetic contribution to the heat capacity within a simple mean-field model. From this analysis we found that this molecular field acting on the rare-earth site increases with the iron concentration, reaching values as large as 48 T for the concentration $x = 6$. A similar analysis of the heat capacity in the ordered phase on the Tb compounds also leads to an enhancement of the molecular field with increasing Fe content. These results allow checking the possible crystal-field parameters for these RFe_xMn_{12-x} compounds.

1. Introduction

In RMn_{12} (R is a rare earth) compounds, the Mn ions are coupled antiferromagnetically, showing Néel temperatures of around 100 K. The magnetic moment arrangement is such that it cancels the effects of eventual R–Mn exchange interactions on the rare-earth site. The magnetic R ions order at low temperatures (below 5 K) only through R–R exchange interactions, leading to two distinct ordering temperatures in the compounds, which is not usual for materials of this type [1, 2]. In most of the studied intermetallic alloys, the 3d subsystem produces a strong exchange field acting on the rare earth and all the magnetic sublattices order at the same time. However, other systems presenting small values of the 3d–4f exchange interaction show two transition temperatures, like RFe_4Al_8 [3], with the same $ThMn_{12}$-type crystal structure.

In these systems, Fe orders between 100 and 200 K in a modulated antiferromagnetic structure that produces a very small molecular field on the rare earth. R becomes slightly polarized (shown by x-ray resonant magnetic scattering) [4]. In the range 10–35 K, the R magnetic ordering takes place, but it does not originate from R–R interactions, which are weak in this series. Other examples of these systems are the rare-earth oxides with perovskite-type crystal structure RMO_3. In $NdFeO_3$ the Fe sublattice orders at 687 K [5]. This ordered Fe sublattice creates an internal exchange field (∼3 T) at the Nd sites so the Nd magnetic moments become polarized (this process is reflected in the specific heat by the appearance of a Schottky anomaly). At sufficiently low temperatures there is competition between the Nd–Nd and the Nd–Fe interaction and a cooperative phase transition takes place, manifested by a sharp λ-type anomaly in the specific heat. Dilution of the antiferromagnetically ordered Fe subsystem enhances the exchange field acting on the rare-earth ions (magnetic vacancies effect) and suppresses the magnetic ordering of the Nd ions, so spin-glass behaviour is found [6].

Fe dilution in RMn_{12} compounds at low ratios can lead to a system with conveniently small 3d–4f exchange interaction to study the competition with 4f–4f interactions and magnetocrystalline anisotropy. RFe_xMn_{12-x} compounds crystallize in the same body-centred tetragonal $ThMn_{12}$-type crystal structure that has one R site and three non-equivalent Mn sites (Wyckoff 8i, 8j and 8f sites), each one occupied by four transition-metal ions. The transition-metal Fe/Mn atoms selectively occupy these sites (most of 8f by Fe and most of 8i by Mn), while both Mn and Fe occupy the sites 8j. Their simple crystal structure offers an interesting opportunity to study both crystalline electric field (CEF) and magnetic interactions [7, 8]. The three magnetic elements exhibit competing planar and axial magnetocrystalline anisotropies and ferromagnetic (F) and antiferromagnetic (AF) exchange interactions with itinerant or localized magnetic character. From the magnetic and neutron scattering work [9] carried out in connection with the present study, we can conclude that the RFe_xMn_{12-x} compounds are AF from $x = 0$ to 6, with Néel temperatures increasing from 120 K for $x = 0$ to around 230 K for $x = 4$, and then decreasing to 220 K for $x = 6$; the compounds with iron composition $x = 8$ are F with Curie temperatures of around 300 K, but an AF arrangement appears only below 150 K at the 8i site in RFe_xMn_{12-x} compounds with a magnetic rare earth R, and at the three transition-metal sites for YFe_xMn_{12-x}. The rare earth orders F at around 5 K in the binary RMn_{12} compounds, but with a small amount of iron, the rare earth no longer orders cooperatively through R–R interactions, but instead a mutual polarization between the R and 3d sublattices appears. Spin-glass behaviour is observed at low temperatures because there is disorder due to the Fe/Mn dilution and frustration of the competing interactions. The introduction of iron leads to a more localized magnetic character of the 3d magnetic moment [10].

Other studies in the series RFe_xMn_{12-x} with R = Ho [11–13], Er and Nd [12, 14] have proposed the existence of several magnetic phase transitions and critical temperatures: F or AF ordering of the 3d sublattice, depending on composition, change from F to (AF + F) orderings at low temperatures (T_N), ordering of the R sublattice at T_C or T_R, making no distinction between the ordering of R and 3d sublattices. Several works have also been reported on the electrical resistivity of polycrystalline RFe_xMn_{12-x} (R = Y, Ho and Er) compounds with $0 \leqslant x \leqslant 9$ over the temperature range 4–400 K [15, 16]. It follows from these works that the anomalous behaviour of the electrical resistivity below T_N, for $x = 0$, is explained invoking electron scattering by substitutional and thermal spin disorder in addition to scattering by phonons and impurities [17].

Heat-capacity measurements provide a valuable method for studying the behaviour of RFe_xMn_{12-x} compounds because the magnetic contribution to the heat capacity is directly related to the energy levels of the three magnetic ions involved. Important information about the ordered state can then be derived from heat-capacity measurements, namely: precisely define the magnetic ordering temperature, the character and nature of the phase transition and, in some cases, from the fit of the heat capacity to a theoretical model, microscopic parameters concerning both CEF and exchange interactions present in the system can be obtained or checked. In addition, a study of the phase diagram of the compound YMn_{12} in terms of different exchange interactions and a numerical Monte Carlo simulation of the temperature dependence of the heat capacity for an Ising model reveal the effect of the 3d exchange competition on the physical properties of these materials.

2. Experimental details

Polycrystalline samples of composition RFe_xMn_{12-x} [R = Gd ($x = 2$, 4 and 6), Tb ($x = 0$, 2, 4, 6 and 8) and Dy ($x = 8$)] were synthesized by induction melting of the constituent elements using an excess of Mn due to the high Mn vapour pressure. These samples were annealed at 1000 °C for 5 d in argon atmosphere. They were subsequently checked for phase purity by x-ray powder diffraction using a high-resolution Seifert-XRD-3000 diffractometer at the University of Oviedo. In the $TbMn_{12}$ sample, β-Mn (12%) and a small amount of Tb_6Mn_{23} (less than 0.5%) were detected, as occurred in the Y and Er compounds [10, 12]. The $R_6(FeMn)_{23}$ phase was not present in the ternary compounds, while the amount of β-Mn decreased with increasing Fe concentration.

The heat capacity $C_p(T)$ was measured in an adiabatic calorimeter based on the heat pulse method at the University of Oviedo. The experimental installation is a commercial adiabatic calorimeter from Termis Ltd [18]. Samples were located in a titanium vessel of 1 cm^3 volume sealed with helium gas inside to improve the heat exchange and reduce the thermal equilibrium times. The adiabaticity is maintained by an inner copper screen, which is controlled by an electronic PID unit that follows the sample temperature with differences smaller than 0.01 K. Another external copper screen is controlled with respect to the inner one. The whole device is in high vacuum provided by a charcoal getter. The sample mass used for the measurements was around 3 g for all the compounds. The absolute accuracy of the equipment, estimated from a measurement with a standard oxygen-free high conductivity

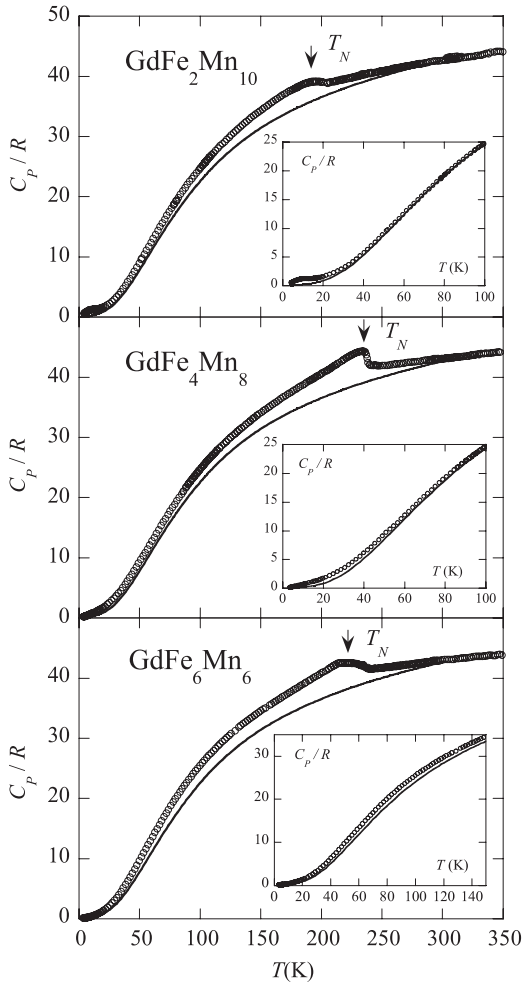

Figure 1. Heat-capacity measurements of $GdFe_xMn_{12-x}$ ($x = 2$, 4 and 6) with the non-magnetic base line (solid line) obtained from $LuFe_{11}Ti$ (see text). The insets are extended views of the low temperature region showing a base line derived from $LuFe_6Mn_6$ that contains the magnetic contribution of the 3d lattice. T_N is the Néel temperature.

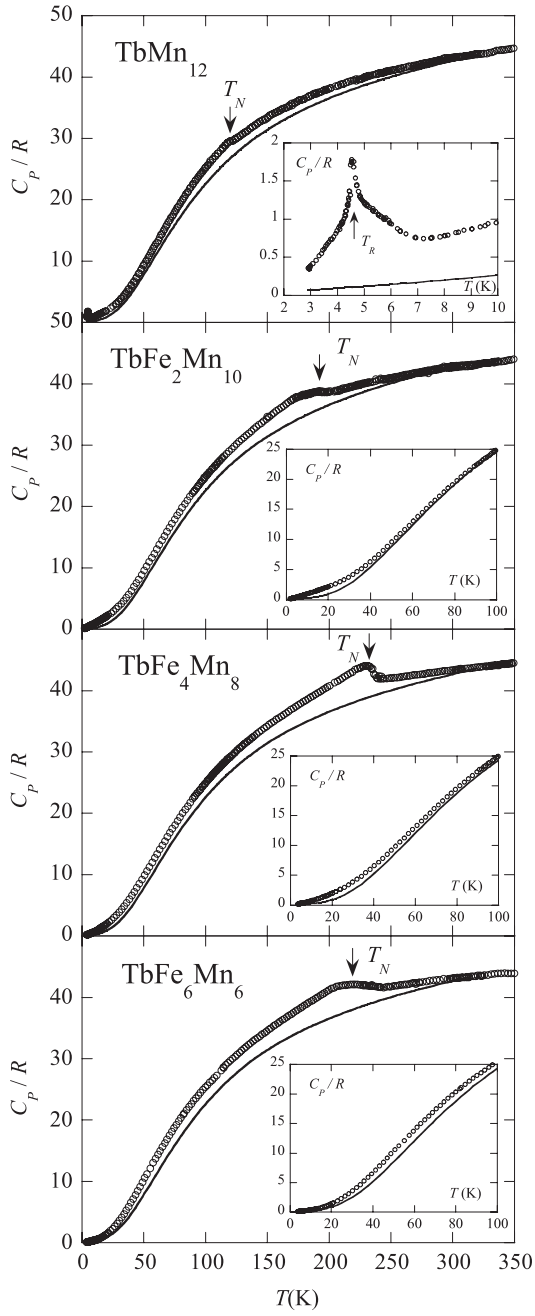

Figure 2. Heat-capacity measurements of $TbFe_xMn_{12-x}$ ($x = 0$, 2, 4 and 6) with the non-magnetic base line (solid line) obtained from $LuFe_{11}Ti$ (see text). The insets are extended views of the low temperature region showing a base line derived from $LuFe_6Mn_6$ that contains the magnetic contribution of the 3d lattice. T_N is the Néel temperature.

copper sample, was better than 0.3% for temperatures higher than 100 K and better than 1.5% for the lowest temperatures (∼3 K) [19].

3. Results and discussion

The heat-capacity (C_p) measurements of RFe_xMn_{12-x} (R = Gd, Tb and Dy) are shown in figures 1–3. For all the compounds a second-order anomaly corresponding to the magnetic ordering of the 3d sublattice is observed in the high temperature regime, and the rare-earth contribution appears at low temperatures.

3.1. Analysis of the magnetic ordering of the 3d sublattice: Monte Carlo simulation

The anomalies at the transition temperature corresponding to the magnetic ordering of the 3d sublattice are very reduced and smoothed (see figures 1–3) owing to the itinerant magnetic character of the 3d electrons, as was previously observed in the YFe_xMn_{12-x} compounds [10, 20]. Taking the ordering temperature at the maximum of the C_p anomaly we obtain the transition temperatures presented in table 1 that are quite close to those found from neutron-diffraction measurements [9].

In order to evaluate the magnetic contribution to the total heat capacity we have taken the heat capacity of $LuFe_{11}Ti$ as the baseline that includes the phonon and electronic contributions up to 300 K [21]. This compound was also

Table 1. Results obtained from heat-capacity measurements of the RFe_xMn_{12-x} series: Néel temperature (T_N); Curie temperature (T_C); rare-earth ordering temperature (T_R); total magnetic entropy from 0 to 300 K (ΔS_{mag}); jump of the specific-heat anomaly (ΔC_{mag}) at the ordering temperature; and molecular field acting on the rare earth at $T = 0$ K. In the case of the $TbFe_xMn_{12-x}$ series this molecular field has been derived in combination with the CEF parameters taken from the literature (see text): set H stands for Hu *et al* [33]; set C for Caciuffo *et al* [34]; and set W for Wang *et al* [35].

	T_N (K)	T_C (K)	T_R (K)	ΔS_{mag} (R f.u.)	Δ_{mag} (R f.u.)	B_{mol} (T)
$GdFe_2Mn_{10}$	197(2)			5.9(1)	3.5(1)	8.0(5)
$GdFe_4Mn_8$	234(1)			6.4(1)	5.5(1)	22(1)
$GdFe_6Mn_6$	223(3)			6.5(1)	4.9(1)	48(3)
$TbMn_{12}$	120(2)		4.5(1)	6.8(1)	2.7(1)	2.0(1) C, 1.6(1) H, 1.5(1) W
$TbFe_2Mn_{10}$	193(2)			6.4(1)	3.5(1)	8(1) H, 8(1) C, 11(1) W
$TbFe_4Mn_8$	232(1)			6.7(1)	5.2(1)	20(2) W, 14(2) H, 12(2) C
$TbFe_6Mn_6$	218(3)			6.8(1)	4.7(1)	35(4) W, 29(4) H, 25(4) C
$TbFe_8Mn_4$		295(5)				
$DyFe_8Mn_4$		300(5)				

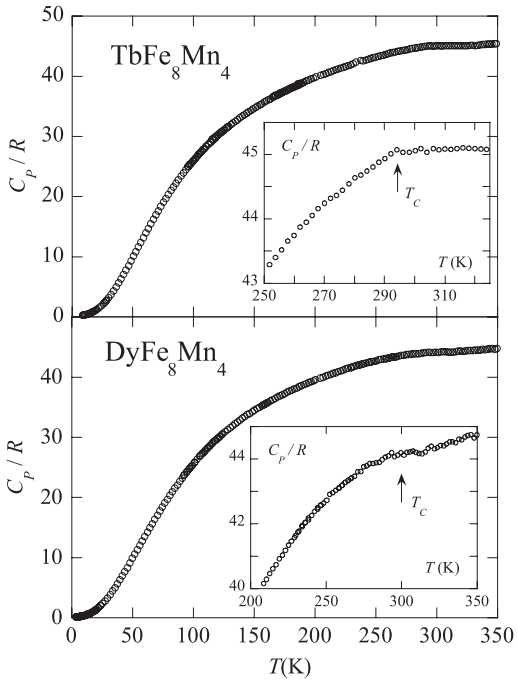

Figure 3. Heat-capacity measurements of RFe_8Mn_4 (R = Tb and Dy). The insets show the high temperature region, T_C is the Curie temperature.

used with success as a baseline to study the YFe_xMn_{12-x} compounds leading to reliable results [10]. In figures 1 and 2 we present, as a continuous line, the heat capacity of $LuFe_{11}Ti$ from 5 to 300 K. From the subtraction of this baseline, the resulting magnetic contribution to the heat capacity, C_{mag}, is determined. The total magnetic entropy enclosed by the anomalies, ΔS_{mag}, is obtained by numerical integration of C_{mag}/T between the lowest measured temperature and 300 K. The low temperature contribution has been estimated extrapolating C_{mag} to 0 K using the Schottky dependence of the heat capacity at low temperatures for all the compounds, except for $TbMn_{12}$ where the spin wave approximation for a ferromagnetic compound has been used. The results, together with the heat-capacity jump at the ordering temperature, ΔC_{mag}, are gathered in table 1.

As expected, the magnetic entropy in RFe_xMn_{12-x} is higher than in the corresponding YFe_xMn_{12-x} compounds. This is due to the rare-earth sublattice contribution to C_p coming from the population of the electronic energy levels of the rare earth and is related to the strength of CEF and the 4f–3d exchange interactions. This additional entropy due to the rare-earth sublattice has been estimated from the theoretical expected values ($S^R_{mag} = R\ln(2J+1) = 2.08R$ for Gd and $2.56R$ for Tb, where R is the ideal gas constant and J is the rare-earth total angular momentum) assuming localized character for the rare-earth electrons. The magnetic entropy of the 3d electrons has been obtained from the difference between the experimental entropies and the estimated values for the rare-earth electrons. The results are similar to the values obtained for the non-magnetic rare-earth compounds of this series [10].

As occurred in the YFe_xMn_{12-x} compounds, the heat-capacity jump ΔC_{mag} at the ordering temperature increases with Fe concentration, reaching a maximum for $x = 4$, and having for this concentration the highest Néel temperatures. In addition, the jump is higher in the compounds with a magnetic rare earth than in the corresponding Y compounds. These features mean that the addition of Fe and the interaction 4f–3d tend to localize the 3d electrons.

Monte Carlo simulations of the system YMn_{12} have been used to obtain the temperature dependence of the heat capacity for a model based on the zero-field Ising Hamiltonian of the compound:

$$\mathcal{H} = -\Sigma_{i,j} J_{ij}\boldsymbol{\sigma}_i\boldsymbol{\sigma}_j = -\Sigma_{i,j} J_{ij}\cos\Theta_{ij} \qquad (1)$$

J_{ij} represents the exchange integral between the atoms i and j, and Θ_{ij} is the angle that forms the directions of their magnetic moments, and the spins σ_i and σ_j can take the values ± 1 (which correspond to a spin $S = 1/2$). This choice for Ising spins implies assuming the directions of the magnetic moments are fixed by crystalline anisotropy. All these assumptions allow us to keep computational efforts within a reasonable limit. Prior to performing the Monte Carlo simulation, we determine the relevant exchange interactions responsible for the magnetic ordering, taking into account the distances between neighbours and relative angles between magnetic moments of the Mn ions

Table 2. Relevant exchange integrals J_i considered between Mn ions for the establishment of the magnetic structure of the compound YMn_{12} (see text). The crystalline sites involved in the interaction, the number of neighbours z, its distance and the ferromagnetic (F) or antiferromagnetic (AF) character of the interaction in the centre of the stability region of the experimentally determined ordering are described by the representation Γ'_{3b} (see figure 4).

Exchange integrals	Crystalline sites	z	Distance (Å)	Type of coupling
J_1	8i–8i	1	2.36	AF
J_2	8i–8j	2	2.65	AF
J_3	8f–8i	4	2.61	F
J_4	8f–8j	4	2.45	AF
J_5	8f–8f	2	2.36	F

at the 8i, 8j and 8f sites in the magnetic structure of YMn_{12}. The analysis taken is explained in the following paragraphs.

YMn_{12} orders antiferromagnetically in the XY basal plane of the tetragonal unit cell. The magnetic structure was solved by testing the different basis functions of the irreducible representations of the $I4/mmm$ (# 139) space group for the propagation vector $\boldsymbol{k} = (1, 0, 0)$. The best agreement was obtained for a magnetic structure that can be described by the irreducible representation Γ'_3 for all the crystallographic sites 8i, 8j and 8f. The four possible combinations of the representation Γ'_3 are labelled as Γ'_{3a}, Γ'_{3b}, Γ'_{3c} and Γ'_{3d}:

$$\begin{aligned}
\Gamma'_{3a} &= (A_{1xy} - A_{5xy})_{8i} + (A_{1xy} - A_{5xy})_{8j} \\
&\quad + (-A_{1x} + A_{5x} + G_{1y} - G_{5y})_{8f} \\
\Gamma'_{3b} &= (-A_{1xy} + A_{5xy})_{8i} + (A_{1xy} - A_{5xy})_{8j} \\
&\quad + (-A_{1x} + A_{5x} + G_{1y} - G_{5y})_{8f} \\
\Gamma'_{3c} &= (A_{1xy} - A_{5xy})_{8i} + (-A_{1xy} + A_{5xy})_{8j} \\
&\quad + (-A_{1x} + A_{5x} + G_{1y} - G_{5y})_{8f} \\
\Gamma'_{3d} &= (A_{1xy} - A_{5xy})_{8i} + (A_{1xy} - A_{5xy})_{8j} \\
&\quad + (A_{1x} - A_{5x} - G_{1y} + G_{5y})_{8f}.
\end{aligned} \tag{2}$$

The symbols G and A label the combinations $\mathbf{S}_1 - \mathbf{S}_2 + \mathbf{S}_3 - \mathbf{S}_4$ and $\mathbf{S}_1 - \mathbf{S}_2 - \mathbf{S}_3 + \mathbf{S}_4$, respectively, according to Bertaut's notation [22]. In this way, $A_{1xy}(A_{5xy})$ means $S_{1x} - S_{2x} + S_{3y} - S_{4y}(S_{5x} - S_{6x} + S_{7y} - S_{8y})$ where the x, y, z atomic coordinates of atoms 1, 2, 3 and 4 for the sites 8i, 8j and 8f are gathered from the International Tables for Crystallography [23] (the coordinates of atoms labelled as 5, 6, 7 and 8 are found from those of 1, 2, 3 and 4 by the translation vector (1/2, 1/2, 1/2), respectively). The combination Γ'_{3b} corresponds to the magnetic ordering determined experimentally from neutron-diffraction experiments in the compound YMn_{12} [10].

A list of the different nearest neighbours of the Mn ions at the 8i, 8j and 8f sites in the magnetic structure of YMn_{12} is given in table 2. The exchange interactions J_1, J_2, ..., J_5 between the different neighbours listed in table 2 are used as parameters to construct a magnetic phase diagram of the system in terms of the possible magnetic orderings. The domain of stability associated with the four different combinations of magnetic modes (corresponding to the Γ'_3 representation) for the sites 8i, 8j and 8f has been determined.

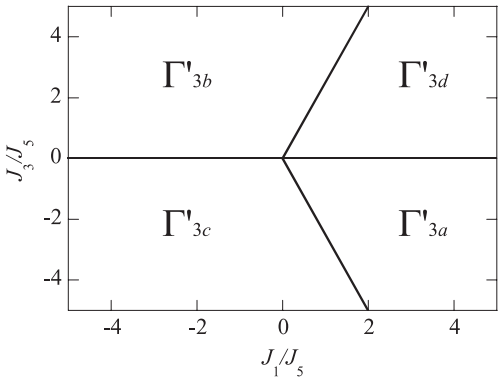

Figure 4. Phase diagram of YMn_{12} for the different combinations of the magnetic modes for the sites 8i, 8j and 8f corresponding to the representation Γ'_3 (defined in equations (2)). The combination Γ'_{3b} corresponds to the magnetic ordering determined experimentally for the compound YMn_{12}. The constraints $J_2 = J_1$ and $J_4 = -J_3$ have been taken for simplicity and the phase diagram is given in terms of the ratios J_1/J_5 and J_3/J_5.

In order to select for a given set of exchange parameters the most energetically favourable magnetic ordering, the exchange energy for the different combinations has been calculated. In figure 4 we represent the domain of stability in terms of the different exchange parameters for the combinations given in equation (2) associated with the representation Γ'_3. For the sake of simplicity, the dimensions of the phase diagram have been reduced by assuming the constraints $J_2 = J_1$ and $J_4 = -J_3$. The exchange integral between 8f magnetic moments along the z axis, J_5, is fixed to be ferromagnetic. The phase diagram represented in figure 4 is given in terms of the ratios J_1/J_5 and J_3/J_5. Magnetic modes obtained from combinations of other representations allowed by symmetry [13, 22] would give the same exchange energies as Γ'_{3b}, but we did not study them as we consider the magnetic moment directions fixed by magnetocrystalline anisotropy. In table 2 we also give the ferromagnetic or antiferromagnetic character of the exchange interactions J_i in the centre of the stability region for the combination Γ'_{3b}. For the 8i atoms there is an AF interaction with the first neighbour of the kind 8i (labelled J_1), AF coupling with the two first neighbours 8j (J_2) and a F interaction with the four first 8f neighbours (J_3). For the 8f sites there is AF coupling between the four first neighbours 8j–8f and F interaction between 8f ions along the z axis.

The heat capacity was calculated by applying the Metropolis Monte Carlo algorithm [24, 25] to the Ising model Hamiltonian equation (1) in a grid with $20 \times 20 \times 20$ unit cells and periodic boundary conditions. For simplicity we assume that the modulus of the five exchange integrals is of the same magnitude ($|J_1| = |J_2| = \cdots = |J_5|$). In figure 5 we plot the magnetic heat capacity obtained by deriving numerically the energy of the system (computed from equation (1)) with respect to the temperature ($C_{\mathrm{mag}} = \mathrm{d}\langle E\rangle/\mathrm{d}T$) and the experimentally measured values of C_{mag} for YMn_{12} [10]. The computed value of the magnetic heat capacity at the transition temperature was $2.12R$, which is in good agreement with the experimentally determined one, $2.26R$ [10]. The temperature axis of the computed curve has been scaled so that

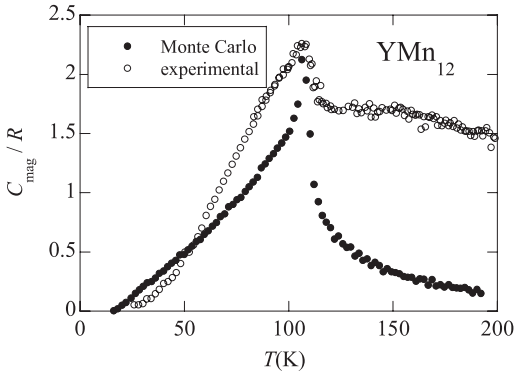

Figure 5. Magnetic heat capacity of YMn_{12} obtained experimentally [10] together with the values determined numerically by applying the Metropolis Monte Carlo algorithm to the Ising model Hamiltonian in a grid with $20 \times 20 \times 20$ unit cells and periodic boundary conditions.

the transition temperature agrees with the experimental value, $T_N = 110(3)$ K [10]. This model–experiment correlation allows us to obtain the magnitude of the exchange interactions: $|J_i| = 43.35k_B$ K. The quantitative attempt using Monte Carlo calculations has proved to be difficult to construct a realistic model of C_p in YMn_{12}. Although the shape of the experimental C_p variation is quite different from the calculated one, two features are worth noting: (i) C_p is almost zero below $T/T_N = 0.25$ with no magnetic contributions, as expected for Ising-type Hamiltonians and (ii) the magnitude of the jump at T_N is quite reduced and seems to be related to the competing interactions of several magnetic 8i, 8j and 8f sites. However, in the paramagnetic region, there is an anomalous contribution to C_p in YMn_{12} that cannot be explained from Monte Carlo simulations within this localized Ising model. This contribution could be attributed to the itinerant magnetic character of the 3d electrons in this material, and the development of spin fluctuations above T_N, as has been observed in the YMn_2 compound [26]. According to Moriya's theory [27] on spin fluctuations for itinerant magnetic materials, additional contributions to C_p would be expected due to an enhancement of spin fluctuations with a wavevector near the propagation vector $\boldsymbol{k} = (1, 0, 0)$ associated with the AF ordering below $T_N = 110$ K exhibited by YMn_{12}. To confirm that this anomalous spin-fluctuation contribution is present in this material, further measurements of C_p are needed to check whether this contribution above T_N would be reduced by the action of an external magnetic field, which suppresses these spin fluctuations that cannot be described in terms of well-defined local moments. In conclusion, from the analysis of the magnetic heat capacity of YMn_{12} within an Ising model, the small value and smoothed dependence of this magnitude seem to be associated with the strong competition of the exchange interactions between the different neighbours (sites 8i, 8j and 8f) separated by distances between 2.36 and 2.65 Å.

3.2. Analysis of the rare-earth contribution to the heat capacity: determining 3d–4f exchange interactions

In the low temperature regime, a λ-type anomaly has been detected at $T_R = 4.5$ K for the binary compound $TbMn_{12}$, corresponding to the cooperative ordering of the rare-earth sublattice (see the top inset in figure 2). Above T_R, a large magnetic contribution still subsists, only a small part of which can be attributed to short-range order in the immediate vicinity of the ordering temperature. In all the compounds with Fe, the rare-earth contribution to the heat capacity appears as a smooth Schottky-like anomaly due to the population of the rare-earth energy levels (see insets of figures 1 and 2). No λ-type anomaly, corresponding to the magnetic ordering of the rare-earth sublattice via 4f–4f interactions, has been detected in the RFe_xMn_{12-x} ternary compounds. This means that there is no long-range order involving 4f electrons, but the rare earth is then polarized due to the 3d–4f interaction, which appears when an imbalance in the 3d sublattices is created by the addition of Fe, in accordance with the results from neutron experiments [9]. Similar types of anomalies have also been found in RFe_4Al_8 compounds [28].

In order to evaluate the rare-earth contribution to the heat capacity we have taken the isostructural compound $LuFe_6Mn_6$, with a non-magnetic rare earth, as the baseline that accounts for the lattice, electronic and AF ordering of the 3d sublattice. This baseline is shown in the insets of figures 1 and 2. To take into consideration the different volumes and magnetic phase transition temperatures between the compounds, a corresponding state law is used. Subtracting the $LuFe_6Mn_6$ baseline, the rare-earth contribution to the heat capacity is obtained and represented in figures 6 and 7.

The heat capacity has been calculated and compared with the experimental results. The Hamiltonian for a rare earth, taking into account the CEF on a tetragonal D_{4h} local symmetry, the molecular field created by the 3d sublattice and also by the 4f sublattice can be written:

$$\begin{aligned}\mathcal{H} &= B_2^0 O_2^0 + B_4^0 O_4^0 + B_4^4 O_4^4 + B_6^0 O_6^0 + B_6^4 O_6^4 \\ &\quad + g_J \mu_B \boldsymbol{J} \cdot (\boldsymbol{B}_{\text{mol}}^{\text{3d–4f}} + \boldsymbol{B}_{\text{mol}}^{\text{4f–4f}}) \\ &= \mathcal{H}_{\text{CEF}} + g_J \mu_B \boldsymbol{J} \cdot \boldsymbol{B}_{\text{mol}}^{\text{3d–4f}}(0) m_{3d}(T) \\ &\quad - g_J^2 \mu_B^2 \lambda^{\text{4f–4f}} \boldsymbol{J} \cdot \langle \boldsymbol{J} \rangle + 0.5 g_J^2 \mu_B^2 \lambda^{\text{4f–4f}} \langle \boldsymbol{J} \rangle^2 \end{aligned} \quad (3)$$

$\mathcal{H}_{\text{CEF}}$ is the CEF Hamiltonian, the CEF parameters are $B_n^m = \theta_n \langle r^n \rangle A_n^m$, where θ_n are the Steven's factors α, β and γ, for $n = 2$, 4 and 6, respectively, O_n^m are the Steven's operators, $\langle r^n \rangle$ is the average of r^n over the radial wavefunction of the 4f electrons [29] and A_n^m are the CEF coefficients. $\boldsymbol{B}_{\text{mol}}^{\text{3d–4f}}(0)$ is the molecular field acting on the rare earth that comes from the 3d sublattice at $T = 0$ K. Its temperature dependence, $m_{3d}(T)$, follows the dependence of the 3d sublattice reduced magnetization, g_J is the Landé factor, μ_B the Bohr magneton and $\boldsymbol{J}$ the total angular momentum of the rare earth. The third term represents the 4f–4f exchange interaction in the molecular-field approximation, being $\lambda^{\text{4f–4f}}$ the molecular-field parameter. The last term corresponds to the self-interaction correction. After diagonalization of the Hamiltonian [30], the free energy has been calculated from the partition function and the magnetic heat capacity has then been derived.

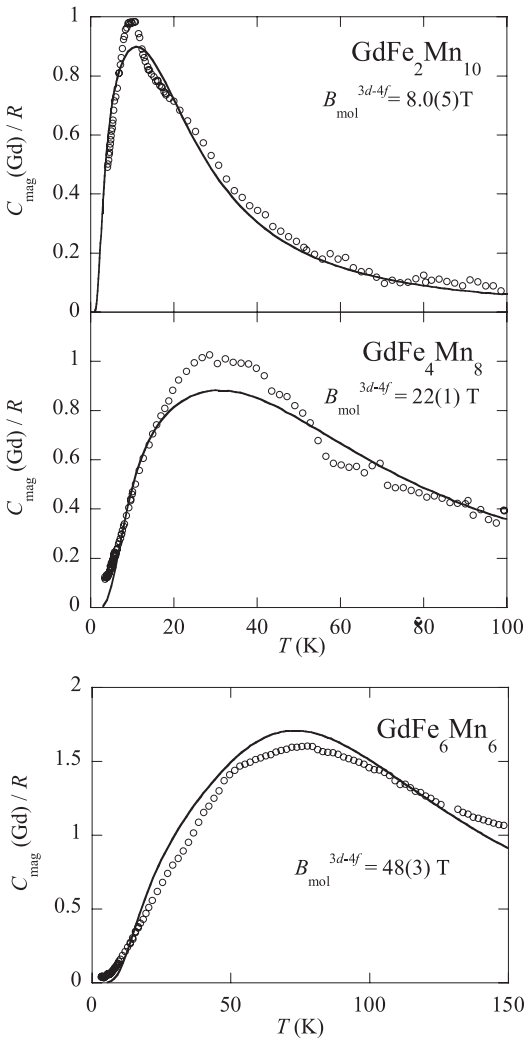

Figure 6. Estimated experimental magnetic contribution of Gd to the heat capacity of $GdFe_xMn_{12-x}$ ($x = 2$, 4 and 6) (points) together with the theoretical calculations (solid lines). B_{mol}^{3d-4f} are the molecular fields derived.

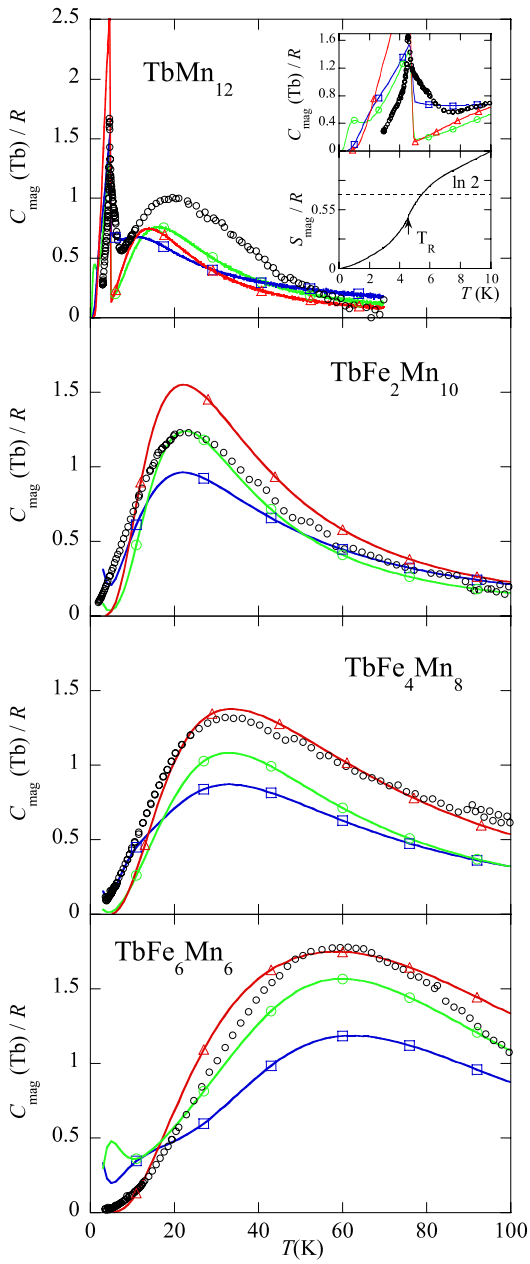

Figure 7. Estimated experimental magnetic contribution of Tb to the heat capacity of $TbFe_xMn_{12-x}$ ($x = 0$, 2, 4 and 6) (points) together with the theoretical calculations using the CEF parameters taken from the literature (see table 3, ○ for set H [33], □ for set C [34], △ for set W [35]) and the molecular field derived in this work (see table 1). The insets show the low temperature region, and the magnetic entropy, S_{mag}, around the rare-earth ordering temperature for $TbMn_{12}$.

(This figure is in colour only in the electronic version)

In the case of Gd compounds ($x = 2$, 4 and 6) (figure 6), the absence of CEF interaction allows us to determine the magnitude of the molecular field. Only the 3d–4f exchange interaction is taken into account, the 4f–4f interaction being negligible. The magnitude of the molecular field has been deduced fitting the magnetic contribution to the heat capacity. For $x = 2$ and 4, the temperature dependence for the molecular field, $m_{3d}(T)$, has been taken to be of Brillouin-type. For $x = 6$, $m_{3d}(T)$ is assumed to follow the temperature dependence of the 8f magnetic moment that polarizes the Gd magnetic moment. This dependence is of linear type, as deduced from neutron experimental data for the Tb and Dy compounds [9]. Fitting the experimental heat capacity with only one free parameter we have calculated the values for the molecular-field coefficient, being $B_{mol}^{3d-4f}(0) = 8.0(5)$ T for $x = 2$; 22(1) T for $x = 4$ and 48(3) T for $x = 6$, as presented in table 1 and figure 6.

In addition to the exchange interactions, in the case of Tb compounds CEF effects must be considered. In lower symmetry systems such as the tetragonal RFe_xMn_{12-x}, the number of CEF parameters (up to 5, see equation (3)) renders the determination of these parameters quite complicated [31, 32]. Until now, due to the difficulty for obtaining RFe_xMn_{12-x} single crystals there is not a realistic determination of CEF parameters in this series. In this way, the available CEF parameters in the literature for isostructural $ThZn_{12}$-type compounds have been tested. Although using information from heat capacity

Table 3. CEF parameters A_n^m (in units of $K a_0^{-n}$ where a_0 is the Bohr radius) taken from the literature and used to calculate the heat capacity for $TbFe_xMn_{12-x}$ series.

	Parameters				
	A_2^0	A_4^0	A_4^4	A_6^0	A_6^4
H [33]	−32.3	−12.4	118	2.56	0.64
C [34]	−106.7	27.8	127.6	−3.6	−24.4
W [35]	−51.8	−5.4	−69.3	0.49	0

alone is not effective in the search of CEF parameters, it allows an easy check to decide whether a set of parameters is appropriate or not. Table 3 summarizes the parameters checked in the calculations. The different sets are identified by the capital letter of the first author. The set of parameters H has been derived by Hu *et al* [33] on a single crystal of $DyFe_{11}Ti$ from magnetization curves. The set C of Caciuffo *et al* [34] has been obtained on $TbMn_4Al_8$ from inelastic neutron scattering experiments, and finally the set W corresponds to the determination made by Wang *et al* [35] on a single crystal of $TbFe_{11}Ti$ from high-field magnetization measurements.

In the case of $TbMn_{12}$, the arrangement of Mn moments is such that they cancel the effects of R–Mn exchange interaction on the rare-earth site, and only the CEF and 4f–4f exchange interactions are significant in the above Hamiltonian (3). The calculation was performed in a self-consistent way until reaching convergence for the mean value of the quantum total angular momentum $\langle \boldsymbol{J} \rangle$. With each set of CEF parameters the molecular-field parameter has been adjusted to account for the experimental magnetic phase transition temperature T_R = 4.5 K (see table 1 or, equivalently, $\lambda^{4f-4f} = 0.22$ T/μ_B for C set; $\lambda^{4f-4f} = 0.18$ T/μ_B for H set and $\lambda^{4f-4f} = 0.17$ T/μ_B for W set). In figure 7 the results of the calculations are presented as continuous lines. All the sets predict a Schottky maximum between 12 and 16 K and the experimental maximum is located at about 20 K. This implies a splitting of the CEF levels slightly larger than those found from the proposed sets H, C and W. Only the set C explains the small shoulder above the transition temperature (see upper inset for $TbMn_{12}$ in figure 7) and the experimental heat-capacity jump at T_R, although there are discrepancies in the low temperature region. The experimental magnetic entropy (see inset 2 in figure 7) has been calculated making the low temperature extrapolation to $T = 0$ K from the lowest measured temperature using the F spin waves dependence for the specific heat ($C_p = AT^{3/2}$). The entropy becomes saturated near 70 K with a value $S = 2.4R$ which is very close to the theoretical one for the total splitting of the ground-state multiplet $J = 6$. This suggests an overall CEF splitting of the order of 70 K, which is quite reduced compared to other hexagonal or tetragonal rare-earth intermetallic systems. This feature clearly indicates that the CEF interaction is fairly small, partly because the magnitude of A_2^0 is not so important compared to that of the high order CEF parameters, which could also play a major role in the magnetic anisotropy of the system. On the other hand, the magnetic entropy of the experimental peak below 5 K is $0.6R$, close to $R \ln 2$, suggesting that a low-lying magnetic doublet is involved in the magnetic ordering.

With the addition of Fe, even in small amounts ($x = 2$), the magnetic ordering transition of the Tb sublattice disappears and only a Schottky contribution (figure 7) coming from the population of the rare-earth energy levels (split by CEF and by the exchange field) is observed. In the case of $x = 2, 4$, where no magnetic order of the rare earth takes place and a spin-glass behaviour has been proposed [9], the exchange field is of local type and appears due to short-range R–3d or R–R correlations. The shoulder of the heat capacity of $TbMn_{12}$ around 6 K does not appear for $x = 2$, 4 and 6, indicating that there is also an abrupt change in the CEF interaction with the addition of iron. The heat capacity for $TbFe_xMn_{12-x}$ ($x = 2$, 4 and 6) has been calculated assuming the above CEF parameters (see table 3) and adjusting a molecular-field coefficient that reproduces the Schottky maximum as shown in figure 7. For $x = 2$, with the lowest Fe concentration studied, none of the sets of CEF parameters explain properly the experimental Schottky anomaly. In particular set H agrees well with the experimental curve above 20 K but predicts a maximum at low temperatures which is not observed, so there is an important discrepancy in the low-lying energy levels for the H and also for the C sets. For $x = 4$ and 6 the maximum of the Schottky anomaly shifts to high temperatures, reflecting the increase of the 3d–4f molecular field (through the magnetic coupling between the 2a (rare earth) and the 8f (Fe) Wyckoff sites) [9], as has been detected in the Gd compounds. For both compounds the set W of CEF parameters gives the best agreement leading to a molecular field lower than the corresponding values obtained for the Gd compounds (see table 1: 20 T for $x = 4$, and 35 T for $x = 6$).

In this series of intermetallic compounds RT_xM_{12-x}, with $ThMn_{12}$-type crystal structure, drastic changes have been found in the CEF parameters depending on the transition metal (T) and also on the stabilizing element (M). Hence in RFe_xTi_{12-x} the leading CEF coefficient A_2^0 is negative and in RCo_xTi_{12-x} positive [36], but in RFe_4Al_8 it is positive and in RMn_4Al_8 negative [34]. The reason for this is that A_2^0 is not the dominant CEF coefficient in this series and small variations in composition lead to a significant change in its value and even to reversing its sign. In this way, the role of the high order CEF parameters cannot be discarded if A_2^0 is not large enough to govern the magnetic anisotropy. In RFe_xMn_{12-x} compounds it seems that one important parameter is A_4^4, which controls the anisotropy in the basal plane: it is positive for compounds with high Mn content, while this CEF parameter decreases its value and reverses its sign for compounds with high Fe content (see tables 1 and 3). Because A_n^m are proportional to the electric field gradient at the R site created mainly by the nearest-neighbour atoms located at the 8j sites, the substitution of Mn by Fe at these 8j sites causes a modification of the CEF. This feature explains the disagreement found in the low temperature region and the difficulty to make extrapolations from other compounds of the series or to use a single set of CEF parameters for all the compounds.

4. Conclusions

While the binary $TbMn_{12}$ compound presents two phase transitions, with well-defined λ-type anomalies and two

independent ordering temperatures associated with the 3d and R sublattices, the thermodynamic behaviour of RFe_xMn_{12-x} (R = Gd, Tb and Dy) gives strong evidence for several effects produced by the Fe introduction: the dilution of the antiferromagnetically ordered Mn subsystem in RMn_{12} breaks the symmetry of the antiferromagnetic arrangement in the 3d sublattice. Accordingly, for low Fe concentrations a small exchange field acting on the rare-earth ions appears to be wiping out the λ-type anomaly [37]. In this way, a competition between the 4f–4f and 3d–4f exchange interactions takes place, leading to the disappearance of the cooperative ordering of the R sublattice, which behaves like a paramagnetic system under an internal exchange field that polarizes the R magnetic moment. We can say that, in this particular situation, the R magnetic moments are so polarized by the 3d magnetic moments that there is no more entropy left to allow for an order–disorder cooperative magnetic phase transition. Finally, the knowledge of the molecular field and CEF parameters is of key importance for determining the temperature dependence of the heat capacity in the ordered phase of RFe_xMn_{12-x}. From the present analysis, the exchange molecular field increases a factor ∼5 with the addition of Fe. The check of all the available CEF parameters of isostructural $ThZn_{12}$-type compounds make us conclude that the weakness of the second-order CEF parameter A_2^0 allows the fourth-order parameter A_4^4 (which is positive (negative) for Mn (Fe)-rich compounds) to play a major role in governing the physical properties of these materials.

Acknowledgments

This work was supported by Projects MAT2008-06542-C04-03 and MAT2007-61621 from MCYT and FEDER. We also wish to thank the FCYT for the financial support given to EA.

References

[1] Desportes J, Givord D, Lemaire R and Nagai H 1977 *Physica* B **86–88** 69
[2] Okamoto N, Nagai H, Yoshie H, Tsujimura A and Hihara T 1987 *J. Magn. Magn. Mater.* **70** 299
[3] Paixão J A, Ramos Silva M, Sørensen S A, Lebech B, Lander G H, Brown P J, Langridge S, Talik E and Gonçalves A P 2000 *Phys. Rev.* B **61** 6176
[4] Langridge S, Paixão J A, Bernhoeft N, Vettier C, Lander G H, Doon Gibbs, Sørensen S A, Stunault A, Wermeille D and Talik E 1999 *Phys. Rev. Lett.* **82** 2187
[5] Bartolomé F, Kuz'min M D, Bartolomé J, Blasco J, García J and Sapiña F 1994 *Solid State Commun.* **91** 177
[6] Bartolomé F, Kuz'min M D, Bartolomé J, Blasco J and García J 1995 *J. Magn. Magn. Mater.* **140–144** 2159
[7] Yang Y C, Kebe B, James W J, Deportes J and Yelon W 1981 *J. Appl. Phys.* **52** 2077
[8] Amako Y, Saoka S, Yoshie H, Nagai H and Adachi K 1995 *J. Phys. Soc. Japan* **64** 1860
[9] Piqué C, Blanco J A, Burriel R, Abad E, Artigas M and Fernández-Díaz M T 2007 *Phys. Rev.* B **75** 224424
[10] Piqué C, Abad E, Blanco J A, Burriel R and Fernández-Díaz M T 2005 *Phys. Rev.* B **71** 174422
[11] Mao W, Yang J, Cheng B and Yang Y 1999 *Solid State Commun.* **109** 655
[12] Morales M, Bacmann M, Wolfers P, Fruchart D and Ouladdiaf B 2001 *Phys. Rev.* B **64** 144426
[13] Yang J B, Yelon W B, James W J, Cai Q S, Eckert D, Handstein A, Müller K H and Yang Y C 2002 *Phys. Rev.* B **65** 064444
[14] Shelyapina M G, Morales M, Bacmann M, Baudelet F, Fruchart D, Giorgetti C, Hlil E K, Krill G and Wolfers P 2004 *J. Alloys Compounds* **368** 84
[15] Stankiewicz J, Bartolomé J and Fruchart D 2002 *Phys. Rev. Lett.* **89** 106602
[16] Stankiewicz J, Bartolomé J and Fruchart D 2003 *Phys. Rev.* B **67** 92409
[17] Stankiewicz J, Bartolomé J, Morales M, Bacmann M and Fruchart D 2001 *J. Appl. Phys.* **90** 5632
[18] Pavese F and Malyshev V M 1994 *Adv. Cryog. Eng.* **40** 119
[19] Abad E 2001 *PhD Thesis* University of Oviedo, Spain
[20] Blanco J A, Gignoux D and Schmitt D 1991 *Phys. Rev.* B **43** 13145
[21] Melero J J 1997 *PhD Thesis* University of Zaragoza, Spain
[22] Bertaut E F 1963 *Magnetism* vol III, ed R Suhl (New York: Academic) p 150
[23] Hahn T (ed) 2002 *International Tables for Crystallography* vol A *Space-group Symmetry* 5th edn (Dordrecht: Kluwer)
[24] Landau D P and Binder K 2000 *A Guide to Monte Carlo Simulations in Statistical Physics* (Cambridge: Cambridge University Press)
[25] Restrepo J and Greneche J M 2005 *Phys. Rev.* B **71** 064406
[26] Okamoto T, Nagata H, Fujii H and Makihara Y 1987 *J. Magn. Magn. Mater.* **70** 139
[27] Moriya T 1985 *Spin Fluctuations in Itinerant Magnetism* (Berlin: Springer)
[28] Hagmusa I H, Brück E, De Boer F R and Buschow K H J 1998 *J. Alloys Compounds* **80** 278
[29] Freeman A J and Desclaux J P 1979 *J. Magn. Magn. Mater.* **12** 11
[30] Piqué C, Burriel R and Bartolomé J 1996 *J. Magn. Magn. Mater.* **154** 71
[31] Blanco J A, Gignoux D and Schmitt D 1992 *Z. Phys.* B **89** 343
[32] Morin P and Blanco J A 1993 *J. Magn. Magn. Mater.* **119** 59
[33] Hu B P, Li H S, Coey J M D and Gavigan J P 1990 *Phys. Rev.* B **41** 2221
[34] Caciuffo R, Amoretti G, Buschow K H J, Moze O, Murani A P and Paci B 1995 *J. Phys.: Condens. Matter* **7** 7981
[35] Wang J L, García-Landa B, Marquina C, Ibarra M R, Yang F M and Wu G H 2003 *Phys. Rev.* B **67** 014417
[36] Kuzmin M D, Richter M and Buschow K H J 2000 *Solid State Commun.* **113** 47
[37] Blanco J A, Gignoux D, Morin P and Schmitt D 1991 *Europhys. Lett.* **15** 671